

# High-repetition-rate, all-reflective optical guiding and electron acceleration in helium using an off-axis axicon

Jiří Šišma<sup>1,2</sup>, Michal Nevřkla<sup>1,2</sup>, Filip Vitha<sup>1,2</sup>, Sebastian Lorenz<sup>1</sup>, Illia Zymak<sup>1</sup>, Alžběta Špádová<sup>1,2</sup>, Andrea Kollárová<sup>1,2</sup>, Matěj Jech<sup>1,3</sup>, Alexandr Jančárek<sup>1,2</sup>, Davorin Peceli<sup>1</sup>, Carlo M. Lazzarini<sup>1</sup>, Leonardo V. N. Goncalves<sup>1</sup>, Gabriele M. Grittani<sup>1</sup>, Sergei V. Bulanov<sup>1</sup>

<sup>1</sup>ELI Beamlines Facility, The Extreme Light Infrastructure ERIC, Za Radnicí 835, Dolní Břežany 25241, Czech Republic

<sup>2</sup>Faculty of Nuclear Sciences and Physical Engineering, Czech Technical University in Prague, Břehová 7, 11519 Prague, Czech Republic

<sup>3</sup>Faculty of Information Technology, Czech Technical University in Prague, Thákurova 9, 16000 Prague 6, Czech Republic

Jaron E. Shrock<sup>4</sup>, Ela Rockafellow<sup>4</sup>, Ari J. Sloss<sup>4</sup>, Bo Miao<sup>4</sup>, Scott W. Hancock<sup>4</sup>, Howard M. Milchberg<sup>4,5</sup>

<sup>4</sup>Institute for Research in Electronics and Applied Physics and Department of Physics, University of Maryland, College Park, Maryland 20742, USA

<sup>5</sup>Department of Electrical and Computer Engineering, University of Maryland, College Park, Maryland 20742, USA

## Abstract

We present recent results on high-power guiding and laser wakefield acceleration (LWFA) in the ELBA beamline at ELI Beamlines, using the L3-HAPLS laser system (13 J, 30 fs, 0.2 Hz). By employing self-waveguiding in a 20 cm plasma channel in helium, we achieved stable acceleration of electron beams to energies approaching 5 GeV. A novel all-reflective optical setup, including an off-axis reflective axicon, enabled efficient acceleration at 0.2 Hz and guiding at repetition rates up to 3.3 Hz. This compact single laser, single compressor implementation of plasma channels for electron acceleration stabilizes electron pointing and enhances energy gain without requiring modifications to the laser system, paving the way for broader adoption of the technology across user facilities.

**Keywords:** Laser WakeField Acceleration; LWFA; plasma channels; high power laser guiding

## 1. Introduction

Laser wakefield acceleration (LWFA) enables compact generation of high-energy electron beams<sup>[1]</sup>, which are driving advances in several fields. LWFA electron beams are being used to develop compact free-electron lasers (FELs) that produce ultrashort, high-brilliance X-ray and infrared radiation<sup>[2–4]</sup>. These electron beams also serve as sources for secondary particles and radiation, including high-quality positron beams<sup>[5,6]</sup>, high energy photons<sup>[7–10]</sup>, and even muons<sup>[11–13]</sup>, enabling applications in fundamental physics<sup>[14,15]</sup>, and medicine<sup>[16,17]</sup>. Furthermore, the extremely high acceleration gradients achievable with LWFA— $10^3$  times higher than in conventional RF accelerators<sup>[18]</sup> allowing acceleration to multi-GeV energies in sub-meter scale plasma<sup>[19–22]</sup>—open the door to next-generation

high-energy particle colliders, potentially reducing the size and cost of future TeV-scale accelerators<sup>[23]</sup>.

The electron energy gain in LWFA is primarily limited by laser diffraction, pulse depletion and dephasing. To overcome diffraction and maximize energy gain, several guiding techniques have been developed. One approach is self-guiding, where laser pulse creates its own plasma channel via relativistic and ponderomotive self-focusing, balancing diffraction and enabling propagation over several Rayleigh lengths<sup>[20,22,24]</sup>. However, it is a nonlinear process highly dependent on plasma density, which can limit controllability, stability and efficiency. In contrast, pre-formed plasma channels, created in advance using methods such as optical field ionization (OFI)<sup>[21,25–38]</sup> or capillary discharge<sup>[19,39–43]</sup>, provide a stable, low-density core for laser guiding. This enables propagation over much longer

Correspondence to: Email: jiri.sisma@eli-beams.eu

distances (tens of centimeters to meters) and supports higher electron energies<sup>[21,36,37,43]</sup>. Pre-formed channels also offer better control over the plasma density profile, matched laser spot size, and overall stability, reducing shot-to-shot fluctuations and improving beam quality<sup>[35,44]</sup>.

The first plasma waveguides were demonstrated in high-density plasma using inverse Bremsstrahlung heating<sup>[45,46]</sup>. However, this method is inefficient and unsuitable for the low plasma densities required for multi-GeV LWFA<sup>[36,37]</sup>, as it cannot achieve the necessary on-axis densities below  $10^{17} \text{ cm}^{-3}$ . Currently, optical-field ionized (OFI) plasma structures have emerged as the most promising approach for forming free-standing plasma waveguides<sup>[21,25–38]</sup>, which are immune to laser damage and can reliably reach the low densities essential for high-energy acceleration<sup>[21,36,37]</sup> using gas jet technology<sup>[34,47,48]</sup>. In contrast, capillary-based waveguides are limited by their fixed geometry and susceptibility to laser-induced damage<sup>[49]</sup>, and inability to reach densities as low as  $\sim 1 \times 10^{17} \text{ cm}^{-3}$ <sup>[43]</sup>. Electron energies of up to 8 GeV have been achieved using capillary discharge waveguides enhanced with auxiliary laser heating<sup>[43]</sup>.

Advances in laser technology have enabled the use of hydrodynamically expanded OFI plasma columns to form plasma waveguides, allowing for longer acceleration lengths and improved control over plasma profiles<sup>[25,27,30,31,33]</sup>. However, at low target gas density, a single femtosecond channel-forming pulse may not create the core and adequately confining cladding of a plasma waveguide structure by itself. Instead, it ionizes a plasma column causing a hydrodynamic expansion with a plasma “core” on axis and neutral density shock expanding outwards. A secondary pulse is required to ionize the neutral density shock to form the “cladding” and establish the refractive index required for guiding<sup>[25,30,31,33]</sup>. Two main techniques have been developed: the “2-Bessel” method<sup>[30]</sup>, which uses a secondary higher-order Bessel beam to ionize the neutral shock of the OFI channel, allowing guiding of a high or low intensity pulse, or “self-waveguiding” technique<sup>[25,31,33]</sup>, which simplifies the process by using the leading edge of an intense pulse to ionize the neutral shock, forming the waveguide structure for itself as it propagates, simultaneously driving the wake. Both methods have recently been implemented with phase front correction<sup>[21,50,51]</sup> to produce high-fidelity Bessel beams, which are crucial for stable and efficient plasma channel formation. Single-stage plasma accelerators have achieved electron energies up to 10 GeV, using nanoparticle-assisted self-guided LWFA with 130 J on target<sup>[22]</sup> and self-waveguiding of the LWFA driver pulse with 18 J<sup>[36]</sup> and 20 J<sup>[37]</sup> on target, resulting in laser-to-electron beam efficiency of at least 30 %<sup>[36]</sup>.

We present a new modification of the self-waveguiding technique that employs post-compressor splitting of the channel-forming pulse from an initially square transverse profile (super-Gaussian in each dimension) femtosecond

laser pulse. This approach primarily relies on reflective optics, thereby avoiding heat deposition in transmissive components and preventing beam distortions caused by B-integral effects in short pulses. For the first time in high-power LWFA experiments, we implemented an off-axis reflective axicon<sup>[52]</sup>, offering straightforward alignment and reduced risk of laser damage compared to traditional on-axis back-reflective configurations<sup>[30,31]</sup>. The all-reflective setup preserved the compressed pulse duration after the axicon and enabled the formation of plasma channels in helium, which requires laser intensities above  $9 \times 10^{15} \text{ W/cm}^2$  for full ionization<sup>[53,54]</sup>. Previous studies have shown that the plasma channel properties of OFI-generated plasmas can be maintained even at kHz repetition rates<sup>[55]</sup>, confirming the suitability of this approach for future high-repetition-rate accelerators and colliders. In our experiments, we implemented the self-waveguiding LWFA scheme of Ref. 21, where 5 GeV electron acceleration was previously demonstrated in hydrogen. Using an all-reflective geometry, we achieved stable optical guiding of high-intensity laser pulses in a 3 cm plasma channel at 3.3 Hz, and, for the first time in helium, we demonstrated electron acceleration to energies up to 5 GeV in a 20 cm plasma channel. The use of helium as the working gas provides a safer and more easily pumped alternative to hydrogen, which was commonly used in similar experiments<sup>[21,35–37]</sup> due to its lower ionization threshold. This work demonstrates that the proposed approach is both adaptable and efficient for laser user facilities where laser system modification is limited by operational constraints, while enabling maximized electron energy gain compared to conventional self-guiding methods. Owing to its single-compressor implementation, the scheme is well suited for future compact muon sources.

## 2. Experimental setup

The experiments were performed at the ELBA (ELectron Beam Accelerator) beamline<sup>[56]</sup> using the L3-HAPLS Ti:sapphire laser system at the ELI Beamlines facility in the Czech Republic. In these experiments, the laser delivered linearly polarized, 30 fs pulses with peak power of 400 TW at central wavelength 810 nm, providing up to 13 J of energy at 0.2 Hz repetition rate, or up to 8 J at 3.3 Hz. The beam had a rectangular super-Gaussian profile with dimensions of  $214 \times 214 \text{ mm}$ .

In Figure 1, the laser beam enters the auxiliary chamber from the left and is first reflected by a high-reflectivity (HR) dielectric mirror<sup>[57]</sup> (M1). Two pick-off mirrors are then used to split small portions of the pulse to form two auxiliary beams: a channel-forming beam and a probe beam.

The main portion of the beam continues to an HR mirror (M2) and a  $20^\circ$  off-axis parabola (OAP) with a 10 m focal length. The reflected beam is directed by mirror M4 through the central aperture of the off-axis axicon, focusing above the gas jet. Mirror M4 also enables fine alignment between

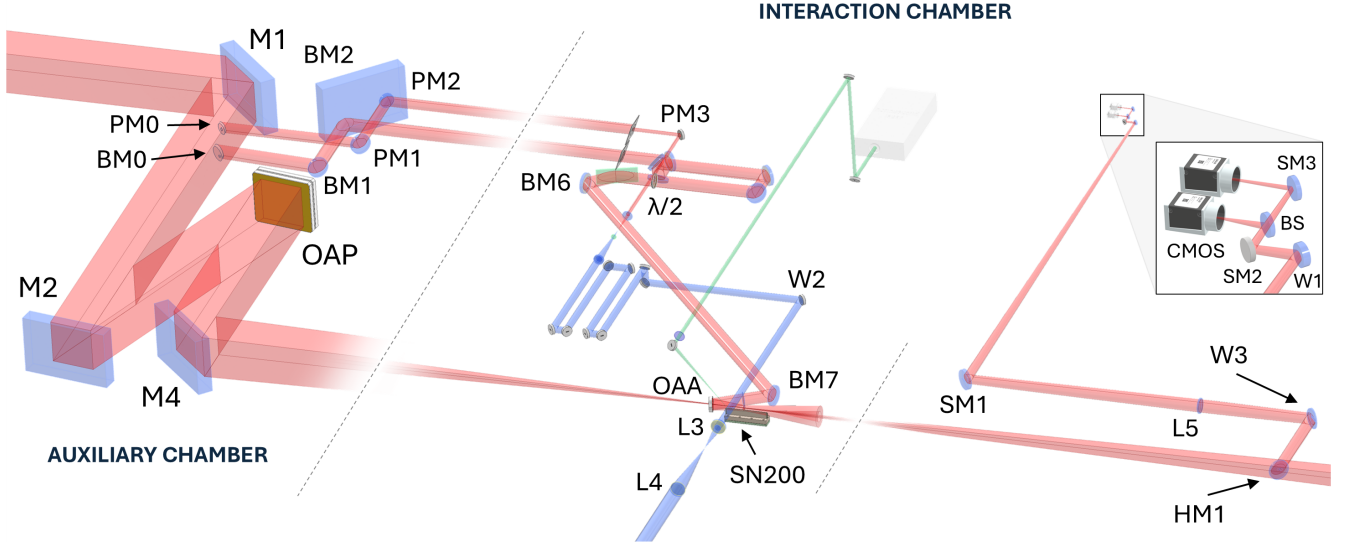


Figure 1: *Experimental setup overview.* The laser beam enters the auxiliary chamber from the left and is reflected by mirror M1. Two pick-off mirrors split small portions of the pulse to form the channel-forming and probe beams, while the main pulse continues as the LWFA drive beam. The channel-forming beam is routed through the auxiliary chamber and directed into the interaction chamber toward the off-axis axicon (OAA) positioned above the gas jet SN200, where it generates the plasma channel. The probe beam is guided through its delay line and diagnostic path, and the drive beam is focused by the off-axis parabola (OAP) into the interaction region for laser wakefield acceleration. The high-power focal-spot and guided-beam diagnostics are shown on the right side of the interaction chamber and include a mirror with a central aperture (HM1), an uncoated wedge (W3), an imaging lens (L5), and a mirror (SM1) that directs the attenuated pulse out of the chamber to CMOS cameras. The green beam path indicates a separate nanosecond laser system used in independent experiments to test alternative injection mechanisms. A detailed description of the setup is provided in the *Experimental setup* section below.

the channel entrance and the drive beam without requiring OAP adjustments, thereby preventing focal spot distortion and ensuring stability during extended operation.

The channel-forming (Bessel) beam is separated by a 45° silver-coated elliptical mirror (BM0) with a 66 mm minor diameter, extracting up to 1.1 J from the initial 13 J pulse. This beam is subsequently guided by a dielectric 4-inch mirror (BM1) and an HR mirror (BM2) into the interaction chamber, connected to the auxiliary chamber by a 6.2 m long beam-transport tube. Within this section, the beam can be apodized using ceramic apertures to achieve the desired diameter and suppress diffraction. All mirrors BM0-BM2 are motorized to allow smooth, remote alignment over long distances, ensuring stability and reproducibility throughout the experiment.

In the remaining beamline (see Figure 2), enhanced silver-coated mirrors (BM3–BM7 and delay-line mirrors) were employed. The single compressor scheme and size of the vacuum chambers constrain the delay to a maximum of 5.6 ns between the LWFA drive pulse and the Bessel beam, adjustable via an 840 mm single-pass delay-line stage. The initially linearly p-polarized channel-forming beam passes through a polarization-changing periscope (BM4–BM5) that rotates its polarization by 90° to work in a reflective attenuator configuration designed for s-polarization. A beam atten-

uator consisting of a half-wave plate ( $\lambda/2$ ) and a reflective femtosecond thin-film polarizer (TFP) was implemented to enable precise control of the Bessel-beam energy<sup>[36,38]</sup>, providing flexibility in tuning the plasma waveguide parameters. The attenuator could be bypassed, allowing operation with only reflective components in the beam path suitable for high-repetition rate operation. Data presented in this paper were taken without the attenuator installed.

Finally, mirrors BM6 and BM7 were used to align a 3-inch reflective 30° off-axis axicon (OAA) with a 3° base angle ( $\approx 105$  mrad approach angle) and a 7 mm central aperture, which allows the LWFA drive beam to couple into the pre-formed density structure above a 20 cm-long supersonic slit-nozzle single-valve gas jet SN200. It is a supersonic slit nozzle system developed at ELI Beamlines<sup>[47]</sup> for long laser-plasma-driven electron acceleration schemes. The nozzle is designed to produce a 20 cm-long region of uniform gas density above the slit, with minimal density variations along the flat-top profile. The system incorporates a gas reservoir and a set of flow deflectors positioned upstream of the nozzle throat to maintain a stable and uniform density distribution, even when operated with a single gas valve connected to the nozzle assembly. This nozzle system differs from previously reported designs<sup>[34,36,48]</sup> in that the gas is supplied through a single valve. This configuration significantly

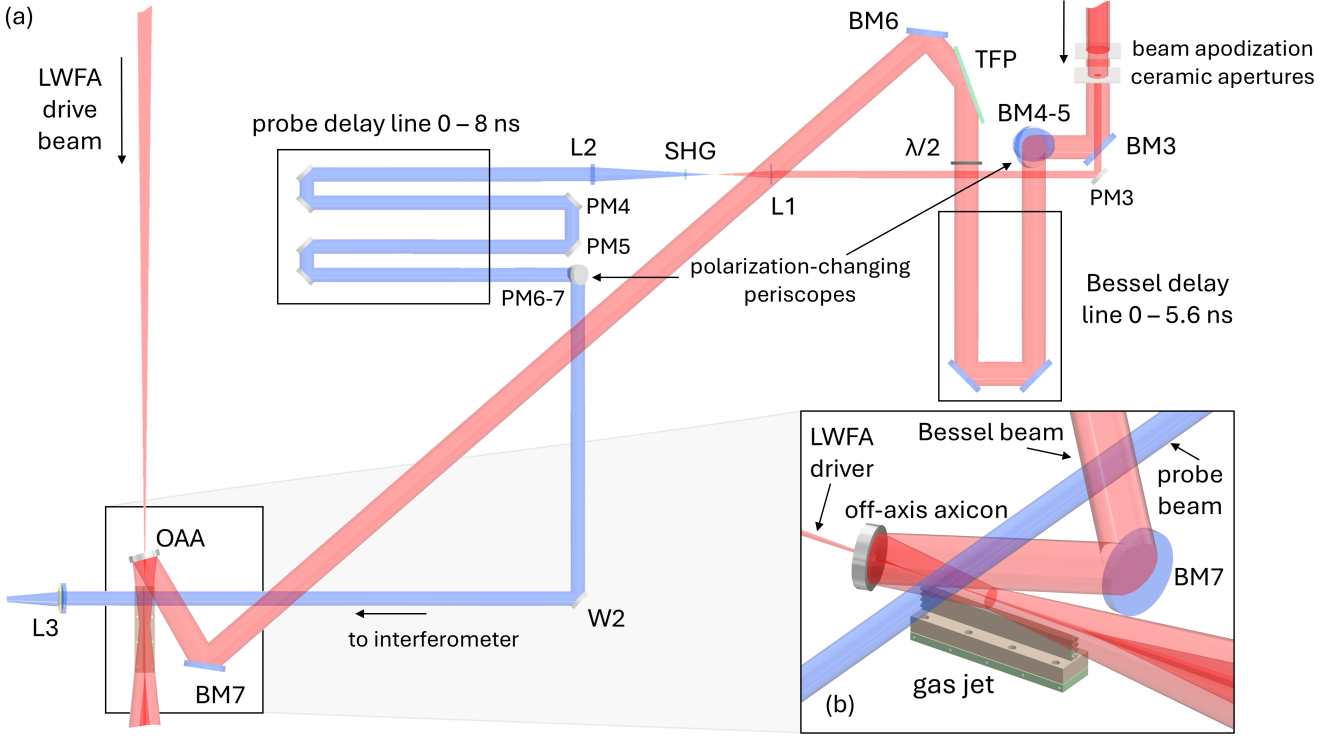


Figure 2: *Schematic layout of the interaction chamber setup for the self-waveguided LWFA experiment.* (a) The final section of the optical system is shown, starting from mirror BM3, where the channel-forming (Bessel) beam enters the chamber, and including all subsequent mirrors BM3–BM7, the periscope, attenuator (half-wave plate,  $\lambda/2$ , and thin-film polarizer, TFP), and delay-line mirrors leading to the off-axis axicon (OAA) positioned above the 20 cm gas jet SN200. The LWFA drive beam passes through the axicon’s central aperture and interacts with the plasma channel formed by the Bessel beam, while the probe beam is directed from its apodization aperture via mirror PM3 to the telescope (lenses L1 and L2) with an SHG BBO crystal, then through a delay line toward the interferometer for diagnostics. (b) A zoomed-in view of the target area, showing the spatial overlap of the channel-forming (Bessel) beam, LWFA drive beam, and probe beam above the gas jet. A detailed description of the setup is provided in the *Experimental setup* section.

simplifies implementation of the system and allows the target to be operated using readily available commercial driver hardware. The trade-off, however, is a comparatively long valve-opening time ( $\approx 10$  ms), which is required for the gas density profile to fully develop prior to the arrival of the laser pulse.

Similarly, the probe beam was extracted from the main laser beam using a 2-inch elliptical, protected silver-coated mirror (PM0). It was then directed by a 4-inch enhanced silver-coated mirror (PM1) and a 3-inch dielectric mirror (PM2) toward the interaction chamber, where it was apodized using a ceramic aperture. The beam was subsequently reflected by a 2-inch protected silver-coated mirror (PM3) into a telescope consisting of a thin lens (L1) and an achromatic lens (L2), transmitting through a beta barium borate (BBO) crystal for second-harmonic generation (SHG) at 800 nm (see Figure 2). For the experimental results discussed in this paper, the fundamental (first harmonic) probe was used exclusively as the diagnostic beam.

The probe beam then passed through a double-pass,

600 mm-long delay line stage, enabling precise timing of the probe pulse with respect to the drive pulse from  $-2$  ns to  $+6$  ns. This allowed temporal scanning of the plasma channel evolution from 0 to 8 ns by adjusting the Bessel beam delay. All mirrors used in the probe beamline (from PM3 to PM7, including those in the delay line) were 2-inch circular protected silver-coated mirrors.

Finally, the probe beam polarization was rotated using a polarization-changing periscope (PM6–PM7), enabling the filtering of p-polarized scattered driver light, and then transmitted through an uncoated wedge (W2) into the interaction region. The transmitted beam was focused by a 3-inch, 200 mm-focal-length achromatic convex lens (L3), forming the first element of a Keplerian telescope that guided the beam out of the chamber through a large-aperture optical window. The beam was then collimated by another 3-inch, 400 mm-focal-length achromatic convex lens (L4) before entering a folded-wave Mach–Zehnder interferometer, where the image was focused onto a complementary metal oxide semiconductor (CMOS) camera with a  $2\times$  magnification.



The scanning interferometer system enables spatial scanning of the probe beam along the gas jet through synchronized motorized control of the wedge W2, the first lens L3, and the entire out-of-chamber interferometer assembly, including lens L4, allowing independent and repeatable positioning along the interaction region.

For the post-interaction diagnostics, we employed a high-power focal-spot and guided-mode diagnostic system consisting of a 4-inch drilled uncoated ultraviolet fused silica (UVFS) mirror (HM1), a 4-inch uncoated wedged (W3) mirror, a 3-inch imaging lens (L5) with a 2000 mm focal length, and a 4-inch protected silver-coated mirror (SM1). Outside the chamber, the beam was reflected by a 1-inch uncoated wedge (W1) and directed by a silver mirror (SM2) toward the first beamsplitter (BS), which sent one portion to a CMOS camera imaging the focal plane. The second image was focused onto another CMOS camera monitoring the guided mode at the exit plane of the waveguide. To prevent detector saturation, absorptive neutral-density filters were placed in front of the cameras for additional attenuation.

The accelerated electron beam passed through a 10 mm central aperture in the first mirror HM1, positioned 3 m downstream from the nozzle exit (corresponding to a 3 mrad divergence). After exiting the chamber through a 1 mm-thick aluminum flange, it propagated toward a 1 mm tungsten slit, composed of 6 cm-thick blocks, placed directly in front of a 50 cm-long slit magnet operating at a uniform magnetic field of 0.6 T. A LANEX screen was mounted at the exit of the magnet and imaged by a CMOS camera equipped with a camera lens and a 546 nm bandpass filter with 10 nm bandwidth for energy-spectrum diagnostics.

We also employed *top-view* and *side-view* fluorescence diagnostics<sup>[34]</sup> consisting of CMOS cameras equipped with camera lenses, motorized neutral-density filter wheels, and a helium line bandpass filter centered at 589 nm with a 10 nm bandwidth. The filter isolated the strong, well-separated helium emission line at 587.6 nm, corresponding to the  $3d \rightarrow 2p$  transition following recombination. To prevent laser light from reaching the detectors and to improve signal quality, infrared (IR) cut filters were placed in front of the cameras (doubled IR cut at 645 nm with  $< 1\%$  averaged transmission in range of 690 – 1070 nm for *side-view* camera and doubled IR cut at 710 nm with  $< 10\%$  averaged transmission in range of 740 – 1200 nm for *top-view* camera). These diagnostics were used for fine alignment of the plasma column above the gas jet and to observe impurities in both the gas sheet and the Bessel beam intensity distribution. The resulting fluorescence signal represents the combined effects of the Bessel beam intensity profile along the propagation and gas density fluctuations or inhomogeneities.

### 3. Laser splitting and focal spot simulations

We performed laser beam-splitting and focal-spot simulations for an ideal super-Gaussian beam using the L3-

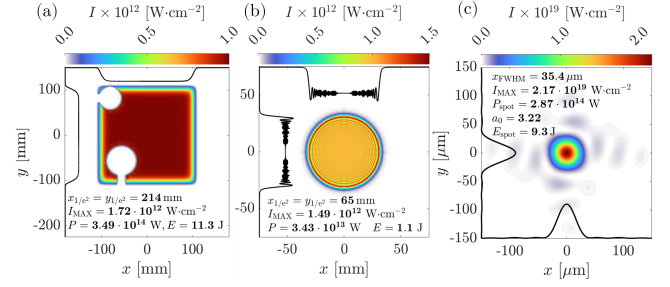


Figure 3: Simulations of laser beam wavefront splitting and focal spot. (a) Wavefront of the LWFA driver beam after the pick-offs at the off-axis parabola (OAP). (b) Wavefront of the channel-forming beam after 12 m of free-space propagation at the axicon surface. (c) Focal spot of the LWFA driver beam (a) on target.

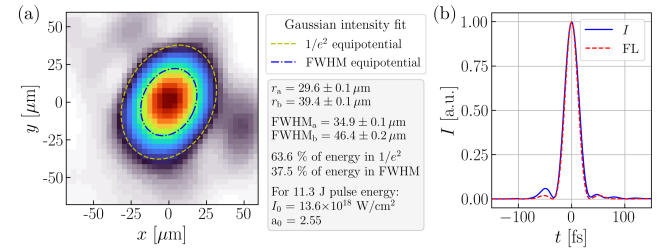


Figure 4: Laser beam measurements. (a) Low-power focal-spot image and corresponding analysis. (b) Laser pulse characterization using SPIDER measurement.

HAPLS laser parameters to compare with the measured focal spots and to estimate the energy distribution in each pulse. Additionally, we simulated the free-space propagation of the Bessel beam to study diffraction-induced distortions after approximately 12 m of propagation. To suppress the resulting diffraction pattern, a serrated aperture can be employed<sup>[58]</sup>. All simulations were carried out using *VirtualLab Fusion 7.0.1* (fast physical-optics simulation software).

In Figure 3, we present simulations of the free-space propagation and focal spot of the LWFA drive beam. For a 13 J, 30.4 fs, 10th-order super-Gaussian pulse, the LWFA driver beam carries 11.3 J of energy (Figure 3(a)), while the channel-forming (Bessel) beam contains 1.1 J. The simulated propagation shows modulation in the near-field of the channel-forming beam intensity due to diffraction effects (Figure 3(b)). The remaining 0.5 J of energy was allocated to the probe beam. The resulting focal spot corresponding to the wavefront (in Figure 3(a)) is shown in Figure 3(c). The expected full width at half maximum (FWHM) is  $\approx 35 \mu\text{m}$ , with a normalized vector potential of  $a_0 = 3.22$ , and a maximum energy in the zeroth diffraction order of 9.3 J, corresponding to 82.3 % of total energy.

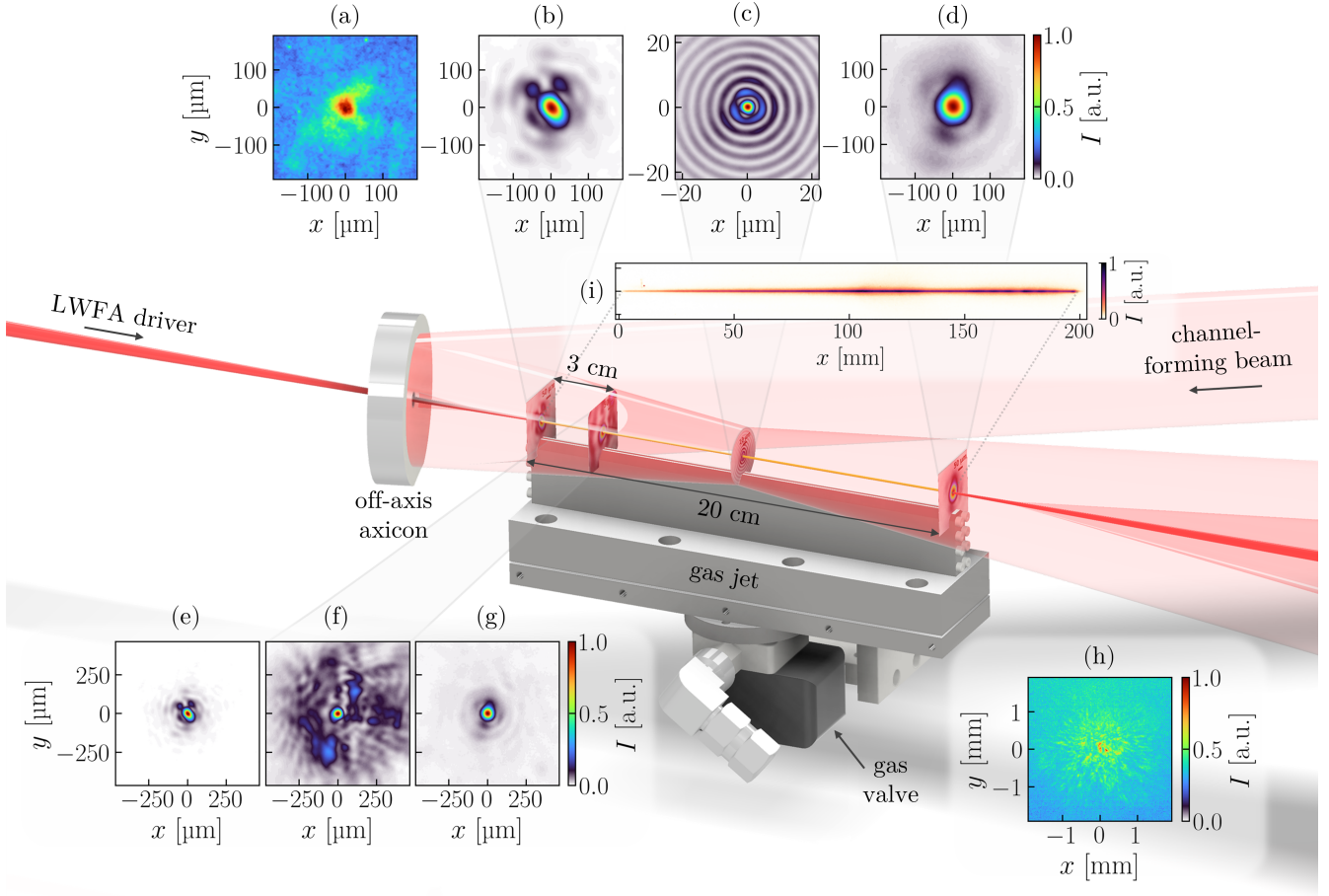


Figure 5: Guiding overview illustrating the interaction between the LWFA drive beam and the channel-forming beam, with the plasma column (yellow) highlighted between the focal plane and the waveguide exit plane above a 20 cm gas jet. (a) High-power focal-spot diagnostic image taken through the gas sheet during active guiding, used for online alignment monitoring. (b) High-power focal spot in vacuum, recorded using the focal-spot diagnostic camera. (c) Bessel beam focal spot, measured with a CMOS camera with  $5\times$  magnification objective. (d) Image of a guided mode exiting 20 cm plasma waveguide acquired by the guided-mode diagnostic camera when the driver beam is successfully coupled into the waveguide. (e) Zoomed-out high-power focal spot image, same as in (b) for comparison with (f) Guided-mode exiting 3 cm plasma waveguide using short 3 cm gas jet (see Figure 6), showing leaky modes<sup>[35]</sup> surrounding the guided beam. (g) Zoomed-out guided mode exiting 20 cm plasma waveguide, same as in (d). (h) Guided-mode image recorded when the driver beam misses the waveguide entrance due to laser-pointing jitter. (i) Top-view fluorescence image of the helium plasma channel generated by the Bessel beam. All images are individually normalized.

#### 4. Experimental results

We have verified pulse compression in the experimental chamber by employing SPIDER (Spectral Phase Interferometry for Direct Electric-Field Reconstruction)<sup>[59]</sup> to measure the femtosecond pulse duration, obtaining 30.4 fs (FWHM), as shown in Figure 4(b). The focal spot was characterized in the low-power regime (L3-HAPLS front-end) by mapping the total energy across the full image, resulting in the distribution presented in Figure 4(a). After noise subtraction, the focal spot was fitted with a Gaussian profile, yielding a minor-axis FWHM of 35  $\mu\text{m}$  and a major-axis FWHM of 46  $\mu\text{m}$ . The overall energy coupling within the beam radius

( $1/e^2$ ) was estimated to be approximately 64 % (7.2 J). For an ideal Gaussian intensity profile, the encircled energy within the  $1/e^2$  radius is approximately 86.5 % of the total energy. The retrieved normalized vector potential was  $a_0 = 2.55$ . Based on performed simulations, the Strehl ratio (defined as the ratio of measured to simulated  $a_0$  in the focal region) was estimated to be 0.79.

##### 4.1. High-repetition-rate, high-power laser guiding

We characterized high-power laser guiding at 0.2 Hz in a 20 cm helium plasma channel (Figure 5) and high-repetition-rate guiding at 3.3 Hz using a 3 cm supersonic slit nozzle

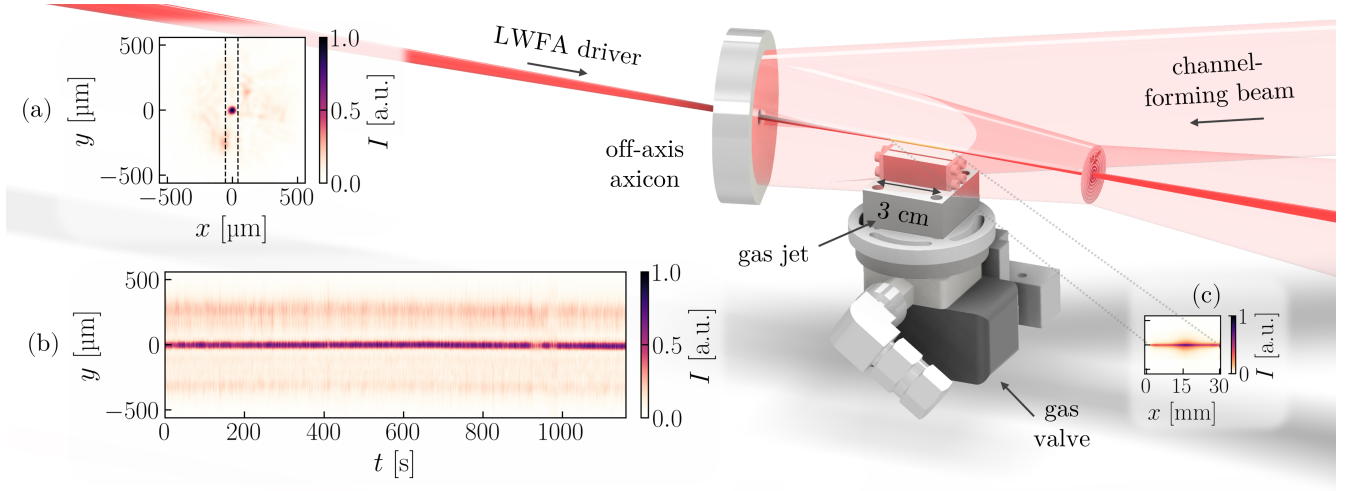


Figure 6: *High-repetition-rate guiding overview illustrating the setup used with a 3 cm slit nozzle.* (a) Guided-mode profile. The lines show the region used to construct the time-evolution plot (b). (b) Evolution of the guided mode in approximately 20 minutes of operation at 3.3 Hz. Each shot is represented by a line-averaged intensity profile taken from the fixed region centered on the guided mode, as indicated in (a) with vertical dashed lines. (c) *Top-view* fluorescence image of the 3 cm helium plasma channel. All images are individually normalized.

(Figure 6). Figures 5(a) and 5(b) show high-power focal-spot images recorded through the gas sheet during active guiding and in vacuum at the focal plane, respectively. The transverse intensity profile of the zeroth-order Bessel beam  $J_0$  is presented in Figure 5(c), yielding a first-zero radius of  $2.83 \pm 0.01 \mu\text{m}$  measured with a  $5\times$  finite-conjugate objective. The guided mode at the 20 cm exit plane is shown in Figure 5(d).

Figures 5(e)-5(g) provide a direct comparison of the focal-spot and guided-mode distributions on a common spatial scale. The guided-mode image in Figure 5(f) was obtained with the 3 cm nozzle (corresponding diagnostics shown in Figure 6). In both the 3 and 20 cm configurations, the guided mode becomes more circularly symmetric relative to the incident focal spot (Figure 5(b)). This behavior is consistent with suppression of higher order mode content via leakage<sup>[31,60,61]</sup> and group velocity walkoff<sup>[35]</sup>. The residual light surrounding the central spot in Figure 5(f) is attributed to leakage from the waveguide.

High-repetition-rate guiding at 3.3 Hz was demonstrated using the 3 cm nozzle, as shown in Figure 6. Figure 6(a) shows the guided-mode image with the region used for line averaging, and Figure 6(b) shows the resulting time evolution over a continuous 20 minute run. The guided mode remains stable throughout the sequence for a  $\approx 250$  TW laser pulse, with no evidence of long-term degradation. The guiding was achieved at a backing pressure of 6 bar.

#### 4.2. Electron acceleration in helium

We achieved electron acceleration in a 20 cm preformed helium plasma channel generated above the supersonic slit

nozzle SN200, operated with a single valve and a 10 ms opening time. The highest-energy shots were obtained with 7.2 J contained within the  $1/e^2$  focal-spot radius (see Figure 4(a)), for delays between  $-1.7$  and  $2.1$  ns between the channel-forming pulse and the LWFA drive pulse, at backing pressures of 37–42 bar. Under these conditions, a 1% nitrogen–helium mixture filled the entire gas jet, leading to broad ionization-injected spectra extending across the full acceleration length. The mean electron energy reached approximately 3.5 GeV, with high-energy features reaching up to  $\sim 5$  GeV (Figure 7). Each spectrum in Figure 7 is shown together with a corresponding pointing image recorded at the entrance of the spectrometer, where the 1 mm slit is indicated by a dashed line. The accelerated electron beams showed the characteristic features of self-waveguided propagation, namely stable pointing and low divergence, here measured to be  $< 5$  mrad, as well as multi-peaked structure from enhancement and suppression of ionization injection along the length of the channel<sup>[21,35]</sup>.

Additional acceleration experiments were carried out using 10% nitrogen–helium and 5% argon–helium mixtures to investigate the influence of dopant concentration and ionization potential on the injection dynamics.

## 5. Discussion

The results demonstrate that the all-reflective optical setup with an off-axis axicon provides stable and efficient guiding of high-power femtosecond laser pulses in helium, achieving both high-repetition-rate operation (3.3 Hz) and multi-GeV electron acceleration (0.2 Hz). The use of reflective components throughout the beamline eliminates thermally induced



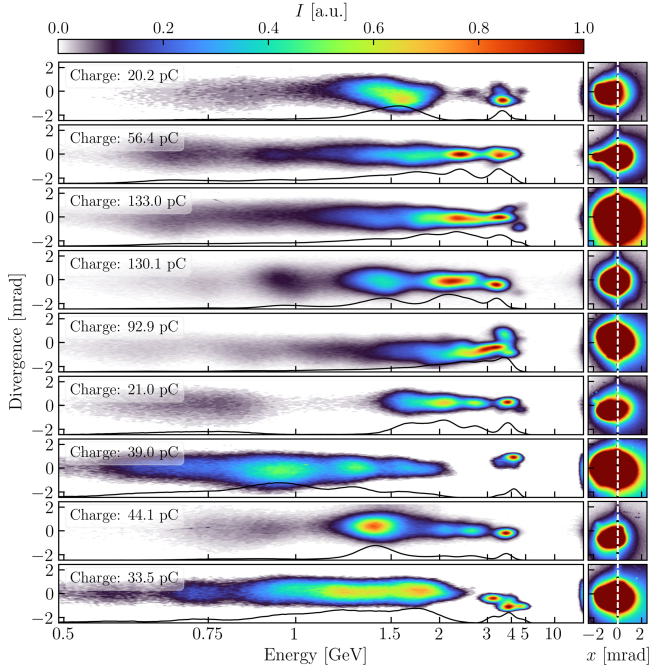


Figure 7: Selection of normalized high-energy electron spectra obtained during acceleration over a 20 cm nozzle at 0.2 Hz with a backing pressure of 37–42 bar. Each spectrum is accompanied by a corresponding pointing image, with the 1 mm spectrometer slit indicated by a dashed line.

distortions typical of transmissive optics and could enhance stability during extended operation. In particular, the off-axis axicon configuration minimizes back-reflections and enables straightforward alignment—a crucial advantage for high-average-power systems and long-duration experimental campaigns.

Compared with previous implementations of self-waveguiding and optical-field-ionized (OFI) plasma channels, our approach streamlines the self-waveguided LWFA scheme, eliminating the past requirements of additional compressors or multi-beam synchronization. The combination of post-compressor beam splitting and all-reflective optics allows the channel-forming beam to be derived directly from the main pulse without compromising pulse duration or spatial phase quality. This technique thus provides an accessible route toward stable and repeatable plasma guiding, fully compatible with existing user-facility laser architectures.

The observed guiding of petawatt-class laser pulses at 3.3 Hz over centimeter-scale distances confirms the robustness of OFI-generated plasma channels even at high repetition rates, consistent with prior low-energy studies. Furthermore, the electron acceleration experiments at 0.2 Hz demonstrate that this method can produce substantial electron energy gain, confirming its suitability for long plasma channels and higher drive-pulse energies. The use of helium, rather than hydrogen, simplifies gas handling and reduces

operational hazards while maintaining efficient ionization and wake excitation.

## 6. Conclusion

We have demonstrated a high-repetition-rate, all-reflective laser guiding and electron acceleration setup employing an off-axis reflective axicon in helium plasma. The system supports stable optical guiding at 3.3 Hz and enables acceleration of electron beams to energies approaching 5 GeV at 0.2 Hz, limited by the available laser parameters. This represents the first implementation of self-waveguiding in helium using a fully reflective optical system. The configuration preserves femtosecond pulse duration, minimizes nonlinear distortions, and enhances reproducibility during extended operation.

The simplicity and robustness of this approach make it highly attractive for deployment in user facilities where modifications to the main laser system are constrained. Beyond serving as a compact and efficient method for high-energy electron acceleration, the presented scheme provides a foundation for future high-repetition-rate plasma accelerators and for the development of laser-driven secondary radiation sources, including compact X-ray and positron sources. Future work will focus on extending the plasma channel length, achieving higher-repetition-rate electron acceleration with petawatt-class lasers, and integrating advanced diagnostics and feedback control for real-time optimization of guiding and acceleration.

## Acknowledgement

This work was supported by the National Science Foundation and Czech Science Foundation under NSF-GACR collaborative Grant No. 2206059 from the Czech Science Foundation Grant No. 22-42963L. This work was supported by the U.S. Department of Energy (DE-SC0015516, LaserNetUS DE-SC0019076/ FWP#SCW1668, and DE-SC0011375), and the Defense Advanced Research Projects Agency (DARPA) under the Muons for Science and Security Program. E. Rockafellow was supported by NSF GRFP (Grant No. DGE 1840340).

## References

1. T. Tajima and J. M. Dawson. Laser electron accelerator. *Phys. Rev. Lett.*, 43:267–270, Jul 1979. doi:10.1103/PhysRevLett.43.267. URL <https://link.aps.org/doi/10.1103/PhysRevLett.43.267>.
2. M. Galletti, R. Assmann, M. E. Couprie, M. Ferrario, L. Giannessi, A. Irman, R. Pompili, and W. Wang. Prospects for free-electron lasers powered by plasma-wakefield-accelerated beams. *Nature Photonics*, 18(8):780–791, 2024. doi:10.1038/s41566-024-01474-3. URL <https://doi.org/10.1038/s41566-024-01474-3>.

3. W. Wang, K. Feng, L. Ke, C. Yu, Y. Xu, R. Qi, Y. Chen, Z. Qin, Z. Zhang, M. Fang, J. Liu, K. Jiang, H. Wang, C. Wang, X. Yang, F. Wu, Y. Leng, J. Liu, R. Li, and Z. Xu. Free-electron lasing at 27 nanometres based on a laser wakefield accelerator. *Nature*, 595(7868):516–520, 2021. doi:10.1038/s41586-021-03678-x. URL <https://doi.org/10.1038/s41586-021-03678-x>.
4. T. André, I. A. Andriyash, A. Loulergue, M. Labat, E. Roussel, A. Ghaith, M. Khojayan, C. Thauray, M. Valléau, F. Briquez, F. Marteau, K. Tavakoli, P. N’Gotta, Y. Dietrich, G. Lambert, V. Malka, C. Benabderrahmane, J. Vétérin, L. Chapuis, T. El Ajjouri, M. Sebdaoui, N. Hubert, O. Marcouillé, P. Berteaud, N. Leclercq, M. El Ajjouri, P. Rommeluère, F. Bouvet, J.-P. Duval, C. Kitegi, F. Blache, B. Mahieu, S. Corde, J. Gautier, K. Ta Phuoc, J. P. Goddet, A. Lestrade, C. Herbeaux, C. Évain, C. Szwaj, S. Bielawski, A. Tafzi, P. Rousseau, S. Smartsev, F. Polack, D. Denettière, C. Bourassin-Bouchet, C. De Oliveira, and M.-E. Couprie. Control of laser plasma accelerated electrons for light sources. *Nature Communications*, 9(1):1334, 2018. doi:10.1038/s41467-018-03776-x. URL <https://doi.org/10.1038/s41467-018-03776-x>.
5. G. Sarri, W. Schumaker, A. Di Piazza, M. Vargas, B. Dromey, M. E. Dieckmann, V. Chvykov, A. Maksimchuk, V. Yanovsky, Z. H. He, B. X. Hou, J. A. Nees, A. G. R. Thomas, C. H. Keitel, M. Zepf, and K. Krushelnick. Table-top laser-based source of femtosecond, collimated, ultrarelativistic positron beams. *Phys. Rev. Lett.*, 110:255002, Jun 2013. doi:10.1103/PhysRevLett.110.255002. URL <https://link.aps.org/doi/10.1103/PhysRevLett.110.255002>.
6. G. Sarri, K. Poder, J. M. Cole, W. Schumaker, A. Di Piazza, B. Reville, T. Dzelzainis, D. Doria, L. A. Gizzi, G. Grittani, S. Kar, C. H. Keitel, K. Krushelnick, S. Kuschel, S. P. D. Mangles, Z. Najmudin, N. Shukla, L. O. Silva, D. Symes, A. G. R. Thomas, M. Vargas, J. Vieira, and M. Zepf. Generation of neutral and high-density electron–positron pair plasmas in the laboratory. *Nature Communications*, 6(1):6747, 2015. doi:10.1038/ncomms7747. URL <https://doi.org/10.1038/ncomms7747>.
7. S. Corde, K. Ta Phuoc, G. Lambert, R. Fitour, V. Malka, A. Rousse, A. Beck, and E. Lefebvre. Femtosecond x rays from laser-plasma accelerators. *Rev. Mod. Phys.*, 85:1–48, Jan 2013. doi:10.1103/RevModPhys.85.1. URL <https://link.aps.org/doi/10.1103/RevModPhys.85.1>.
8. W. Yan, C. Fruhling, G. Golovin, D. Haden, J. Luo, P. Zhang, B. Zhao, J. Zhang, C. Liu, M. Chen, S. Chen, S. Banerjee, and D. Umstadter. High-order multiphoton thomson scattering. *Nature Photonics*, 11(8):514–520, 2017. doi:10.1038/nphoton.2017.100. URL <https://doi.org/10.1038/nphoton.2017.100>.
9. M. Mirzaie, C. I. Hojbota, D. Y. Kim, V. B. Pathak, T. G. Pak, C. M. Kim, H. W. Lee, J. W. Yoon, S. K. Lee, Y. J. Rhee, M. Vranic, Ó. Amaro, K. Y. Kim, J. H. Sung, and C. H. Nam. All-optical nonlinear compton scattering performed with a multi-petawatt laser. *Nature Photonics*, 18(11):1212–1217, 2024. doi:10.1038/s41566-024-01550-8. URL <https://doi.org/10.1038/s41566-024-01550-8>.
10. J. M. Cole, K. T. Behm, E. Gerstmayr, T. G. Blackburn, J. C. Wood, C. D. Baird, M. J. Duff, C. Harvey, A. Ilderton, A. S. Joglekar, K. Krushelnick, S. Kuschel, M. Marklund, P. McKenna, C. D. Murphy, K. Poder, C. P. Ridgers, G. M. Samarin, G. Sarri, D. R. Symes, A. G. R. Thomas, J. Warwick, M. Zepf, Z. Najmudin, and S. P. D. Mangles. Experimental evidence of radiation reaction in the collision of a high-intensity laser pulse with a laser-wakefield accelerated electron beam. *Phys. Rev. X*, 8:011020, Feb 2018. doi:10.1103/PhysRevX.8.011020. URL <https://link.aps.org/doi/10.1103/PhysRevX.8.011020>.
11. W. Dreesen, J. A. Green, M. Browder, J. Wood, D. Schwellenbach, T. Ditmire, G. Tiwari, and C. Wagner. Detection of petawatt laser-induced muon source for rapid high-z material detection. pages 1–6, 2014. doi:10.1109/NSSMIC.2014.7431088.
12. F. Zhang, L. Deng, Y. Ge, J. Wen, B. Cui, K. Feng, H. Wang, C. Wu, Z. Pan, H. Liu, Z. Deng, Z. Zhang, L. Chen, D. Yan, L. Shan, Z. Yuan, C. Tian, J. Qian, J. Zhu, Y. Xu, Y. Yu, X. Zhang, L. Yang, W. Zhou, Y. Gu, W. Wang, Y. Leng, Z. Sun, and R. Li. Proof-of-principle demonstration of muon production with an ultrashort high-intensity laser. *Nature Physics*, 21(7):1050–1056, 2025. doi:10.1038/s41567-025-02872-2. URL <https://doi.org/10.1038/s41567-025-02872-2>.
13. D. Terzani, S. Kisiov, S. Greenberg, L. Le Pottier, M. Mironova, A. Picksley, J. Stackhouse, Hai-En Tsai, R. Li, E. Rockafellow, B. Miao, J. E. Shrock, T. Heim, M. Garcia-Sciveres, C. Benedetti, J. Valentine, H. M. Milchberg, K. Nakamura, A. J. Gonsalves, J. van Tilborg, C. B. Schroeder, E. Esarey, and C. G. R. Geddes. Measurement of directional muon beams generated at the berkeley lab laser accelerator. *Phys. Rev. Accel. Beams*, 28:103401, Oct 2025. doi:10.1103/kxjr-h7zs. URL <https://link.aps.org/doi/10.1103/kxjr-h7zs>.
14. K. Poder, M. Tamburini, G. Sarri, A. Di Piazza, S. Kuschel, C. D. Baird, K. Behm, S. Bohlen, J. M. Cole, D. J. Corvan, M. Duff, E. Gerstmayr, C. H. Keitel, K. Krushelnick, S. P. D. Mangles, P. McKenna, C. D. Murphy, Z. Najmudin, C. P. Ridgers, G. M. Samarin, D. R. Symes, A. G. R. Thomas, J. Warwick, and M. Zepf. Experimental signatures of the quantum nature of radiation reaction in the field of an ultraintense laser. *Phys. Rev. X*, 8:031004, Jul

2018. doi:10.1103/PhysRevX.8.031004. URL <https://link.aps.org/doi/10.1103/PhysRevX.8.031004>.
15. A. Gonoskov, T. G. Blackburn, M. Marklund, and S. S. Bulanov. Charged particle motion and radiation in strong electromagnetic fields. *Rev. Mod. Phys.*, 94:045001, Oct 2022. doi:10.1103/RevModPhys.94.045001. URL <https://link.aps.org/doi/10.1103/RevModPhys.94.045001>.
16. T. Brümmer, A. Debus, R. Pausch, J. Osterhoff, and F. Grüner. Design study for a compact laser-driven source for medical x-ray fluorescence imaging. *Phys. Rev. Accel. Beams*, 23:031601, Mar 2020. doi:10.1103/PhysRevAccelBeams.23.031601. URL <https://link.aps.org/doi/10.1103/PhysRevAccelBeams.23.031601>.
17. L. Labate, D. Palla, D. Panetta, F. Avella, F. Baffigi, F. Brandi, F. Di Martino, L. Fulgentini, A. Giulietti, P. Köster, D. Terzani, P. Tomassini, C. Traino, and L. A. Gizzi. Toward an effective use of laser-driven very high energy electrons for radiotherapy: Feasibility assessment of multi-field and intensity modulation irradiation schemes. *Scientific Reports*, 10(1):17307, 2020. doi:10.1038/s41598-020-74256-w. URL <https://doi.org/10.1038/s41598-020-74256-w>.
18. A. Degiovanni, W. Wuensch, and J. Giner Navarro. Comparison of the conditioning of high gradient accelerating structures. *Phys. Rev. Accel. Beams*, 19:032001, Mar 2016. doi:10.1103/PhysRevAccelBeams.19.032001. URL <https://link.aps.org/doi/10.1103/PhysRevAccelBeams.19.032001>.
19. W. P. Leemans, B. Nagler, A. J. Gonsalves, Cs. Tóth, K. Nakamura, C. G. R. Geddes, E. Esarey, C. B. Schroeder, and S. M. Hooker. GeV electron beams from a centimetre-scale accelerator. *Nature Physics*, 2(10):696–699, 2006. doi:10.1038/nphys418. URL <https://doi.org/10.1038/nphys418>.
20. C. E. Clayton, J. E. Ralph, F. Albert, R. A. Fonseca, S. H. Glenzer, C. Joshi, W. Lu, K. A. Marsh, S. F. Martins, W. B. Mori, A. Pak, F. S. Tsung, B. B. Pollock, J. S. Ross, L. O. Silva, and D. H. Froula. Self-guided laser wakefield acceleration beyond 1 gev using ionization-induced injection. *Phys. Rev. Lett.*, 105:105003, Sep 2010. doi:10.1103/PhysRevLett.105.105003. URL <https://link.aps.org/doi/10.1103/PhysRevLett.105.105003>.
21. B. Miao, J. E. Shrock, L. Feder, R. C. Hollinger, J. Morrison, R. Nedbailo, A. Picksley, H. Song, S. Wang, J. J. Rocca, and H. M. Milchberg. Multi-gev electron bunches from an all-optical laser wakefield accelerator. *Phys. Rev. X*, 12:031038, Sep 2022. doi:10.1103/PhysRevX.12.031038. URL <https://link.aps.org/doi/10.1103/PhysRevX.12.031038>.
22. C. Aniculaesei, T. Ha, S. Yoffe, L. Labun, S. Milton, E. McCary, M. M. Spinks, H. J. Quevedo, O. Z. Labun, R. Sain, A. Hannasch, R. Zgadzaj, I. Pagano, J. A. Franco-Altamirano, M. L. Ringuette, E. Gaul, S. V. Luedtke, G. Tiwari, B. Ersfeld, E. Brunetti, H. Ruhl, T. Ditmire, S. Bruce, M. E. Donovan, M. C. Downer, D. A. Jaroszynski, and B. M. Hegelich. The acceleration of a high-charge electron bunch to 10 gev in a 10-cm nanoparticle-assisted wakefield accelerator. *Matter and Radiation at Extremes*, 9(1):014001, 11 2023. ISSN 2468-2047. doi:10.1063/5.0161687. URL <https://doi.org/10.1063/5.0161687>.
23. C. B. Schroeder, E. Esarey, C. G. R. Geddes, C. Benedetti, and W. P. Leemans. Physics considerations for laser-plasma linear colliders. *Phys. Rev. ST Accel. Beams*, 13:101301, Oct 2010. doi:10.1103/PhysRevSTAB.13.101301. URL <https://link.aps.org/doi/10.1103/PhysRevSTAB.13.101301>.
24. H. T. Kim, K. H. Pae, H. J. Cha, I. J. Kim, T. J. Yu, J. H. Sung, S. K. Lee, T. M. Jeong, and J. Lee. Enhancement of electron energy to the multi-gev regime by a dual-stage laser-wakefield accelerator pumped by petawatt laser pulses. *Phys. Rev. Lett.*, 111:165002, Oct 2013. doi:10.1103/PhysRevLett.111.165002. URL <https://link.aps.org/doi/10.1103/PhysRevLett.111.165002>.
25. A. Morozov, A. Goltsov, Q. Chen, M. Scully, and S. Suckewer. Ionization assisted self-guiding of femtosecond laser pulses. *Physics of Plasmas*, 25(5):053110, 05 2018. ISSN 1070-664X. doi:10.1063/1.5021795. URL <https://doi.org/10.1063/1.5021795>.
26. N. Lemos, L. Cardoso, J. Geada, G. Figueira, F. Albert, and J. M. Dias. Guiding of laser pulses in plasma waveguides created by linearly-polarized femtosecond laser pulses. *Scientific Reports*, 8(1):3165, 2018. doi:10.1038/s41598-018-21392-z. URL <https://doi.org/10.1038/s41598-018-21392-z>.
27. R. J. Shalloo, C. Arran, L. Corner, J. Holloway, J. Jonnerby, R. Walczak, H. M. Milchberg, and S. M. Hooker. Hydrodynamic optical-field-ionized plasma channels. *Phys. Rev. E*, 97:053203, May 2018. doi:10.1103/PhysRevE.97.053203. URL <https://link.aps.org/doi/10.1103/PhysRevE.97.053203>.
28. S. Smartsev, C. Caizergues, K. Oubrierie, J. Gautier, J.-P. Goddet, A. Tafzi, K. Ta Phuoc, V. Malka, and C. Thauray. Axiaparabola: a long-focal-depth, high-resolution mirror for broadband high-intensity lasers. *Opt. Lett.*, 44(14):3414–3417, Jul 2019. doi:10.1364/OL.44.003414. URL <https://opg.optica.org/ol/abstract.cfm?URI=ol-44-14-3414>.
29. R. J. Shalloo, C. Arran, A. Picksley, A. von Boetticher, L. Corner, J. Holloway, G. Hine, J. Jonnerby, H. M. Milchberg, C. Thornton, R. Walczak, and S. M. Hooker. Low-density hydrodynamic optical-field-ionized plasma channels generated with an axicon



- lens. *Phys. Rev. Accel. Beams*, 22:041302, Apr 2019. doi:10.1103/PhysRevAccelBeams.22.041302. URL <https://link.aps.org/doi/10.1103/PhysRevAccelBeams.22.041302>.
30. B. Miao, L. Feder, J. E. Shrock, A. Goffin, and H. M. Milchberg. Optical guiding in meter-scale plasma waveguides. *Phys. Rev. Lett.*, 125:074801, Aug 2020. doi:10.1103/PhysRevLett.125.074801. URL <https://link.aps.org/doi/10.1103/PhysRevLett.125.074801>.
  31. L. Feder, B. Miao, J. E. Shrock, A. Goffin, and H. M. Milchberg. Self-waveguiding of relativistic laser pulses in neutral gas channels. *Phys. Rev. Res.*, 2:043173, Nov 2020. doi:10.1103/PhysRevResearch.2.043173. URL <https://link.aps.org/doi/10.1103/PhysRevResearch.2.043173>.
  32. A. Picksley, A. Alejo, J. Cowley, N. Bourgeois, L. Corner, L. Feder, J. Holloway, H. Jones, J. Jonnerby, H. M. Milchberg, L. R. Reid, A. J. Ross, R. Walczak, and S. M. Hooker. Guiding of high-intensity laser pulses in 100-mm-long hydrodynamic optical-field-ionized plasma channels. *Phys. Rev. Accel. Beams*, 23:081303, Aug 2020. doi:10.1103/PhysRevAccelBeams.23.081303. URL <https://link.aps.org/doi/10.1103/PhysRevAccelBeams.23.081303>.
  33. A. Picksley, A. Alejo, R. J. Shalloo, C. Arran, A. von Boetticher, L. Corner, J. A. Holloway, J. Jonnerby, O. Jakobsson, C. Thornton, R. Walczak, and S. M. Hooker. Meter-scale conditioned hydrodynamic optical-field-ionized plasma channels. *Phys. Rev. E*, 102:053201, Nov 2020. doi:10.1103/PhysRevE.102.053201. URL <https://link.aps.org/doi/10.1103/PhysRevE.102.053201>.
  34. J. E. Shrock, B. Miao, L. Feder, and H. M. Milchberg. Meter-scale plasma waveguides for multi-gev laser wakefield acceleration. *Physics of Plasmas*, 29(7):073101, 07 2022. ISSN 1070-664X. doi:10.1063/5.0097214. URL <https://doi.org/10.1063/5.0097214>.
  35. J. E. Shrock, E. Rockafellow, B. Miao, M. Le, R. C. Hollinger, S. Wang, A. J. Gonsalves, A. Picksley, J. J. Rocca, and H. M. Milchberg. Guided mode evolution and ionization injection in meter-scale multi-gev laser wakefield accelerators. *Phys. Rev. Lett.*, 133:045002, Jul 2024. doi:10.1103/PhysRevLett.133.045002. URL <https://link.aps.org/doi/10.1103/PhysRevLett.133.045002>.
  36. E. Rockafellow, B. Miao, J. E. Shrock, A. Sloss, M. S. Le, S. W. Hancock, S. Zahedpour, R. C. Hollinger, S. Wang, J. King, P. Zhang, J. Šišma, G. M. Grittani, R. Versaci, D. F. Gordon, G. J. Williams, B. A. Reagan, J. J. Rocca, and H. M. Milchberg. Development of a high charge 10 gev laser electron accelerator. *Physics of Plasmas*, 32(5):053102, 05 2025. ISSN 1070-664X. doi:10.1063/5.0265640. URL <https://doi.org/10.1063/5.0265640>.
  37. A. Picksley, J. Stackhouse, C. Benedetti, K. Nakamura, H. E. Tsai, R. Li, B. Miao, J. E. Shrock, E. Rockafellow, H. M. Milchberg, C. B. Schroeder, J. van Tilborg, E. Esarey, C. G. R. Geddes, and A. J. Gonsalves. Matched guiding and controlled injection in dark-current-free, 10-gev-class, channel-guided laser-plasma accelerators. *Phys. Rev. Lett.*, 133:255001, Dec 2024. doi:10.1103/PhysRevLett.133.255001. URL <https://link.aps.org/doi/10.1103/PhysRevLett.133.255001>.
  38. B. Miao, E. Rockafellow, J. E. Shrock, S. W. Hancock, D. Gordon, and H. M. Milchberg. Benchmarking of hydrodynamic plasma waveguides for multi-gev laser-driven electron acceleration. *Phys. Rev. Accel. Beams*, 27:081302, Aug 2024. doi:10.1103/PhysRevAccelBeams.27.081302. URL <https://link.aps.org/doi/10.1103/PhysRevAccelBeams.27.081302>.
  39. N. A. Bobrova, A. A. Esaulov, J.-I. Sakai, P. V. Sasorov, D. J. Spence, A. Butler, S. M. Hooker, and S. V. Bulanov. Simulations of a hydrogen-filled capillary discharge waveguide. *Phys. Rev. E*, 65:016407, Dec 2001. doi:10.1103/PhysRevE.65.016407. URL <https://link.aps.org/doi/10.1103/PhysRevE.65.016407>.
  40. A. Butler, D. J. Spence, and S. M. Hooker. Guiding of high-intensity laser pulses with a hydrogen-filled capillary discharge waveguide. *Phys. Rev. Lett.*, 89:185003, Oct 2002. doi:10.1103/PhysRevLett.89.185003. URL <https://link.aps.org/doi/10.1103/PhysRevLett.89.185003>.
  41. S. Karsch, J. Osterhoff, A. Popp, T. P. Rowlands-Rees, Z. Major, M. Fuchs, B. Marx, R. Hörlein, K. Schmid, L. Veisz, S. Becker, U. Schramm, B. Hidding, G. Pretzler, D. Habs, F. Grüner, F. Krausz, and S. M. Hooker. Gev-scale electron acceleration in a gas-filled capillary discharge waveguide. *New Journal of Physics*, 9(11):415, nov 2007. doi:10.1088/1367-2630/9/11/415. URL <https://doi.org/10.1088/1367-2630/9/11/415>.
  42. T. P. Rowlands-Rees, C. Kamperidis, S. Kneip, A. J. Gonsalves, S. P. D. Mangles, J. G. Gallacher, E. Brunetti, T. Ibbotson, C. D. Murphy, P. S. Foster, M. J. V. Streeter, F. Budde, P. A. Norreys, D. A. Jaroszynski, K. Krushelnick, Z. Najmudin, and S. M. Hooker. Laser-driven acceleration of electrons in a partially ionized plasma channel. *Phys. Rev. Lett.*, 100:105005, Mar 2008. doi:10.1103/PhysRevLett.100.105005. URL <https://link.aps.org/doi/10.1103/PhysRevLett.100.105005>.
  43. A. J. Gonsalves, K. Nakamura, J. Daniels, C. Benedetti, C. Pieronek, T. C. H. de Raadt, S. Steinke, J. H. Bin, S. S. Bulanov, J. van Tilborg, C. G. R. Geddes, C. B. Schroeder, Cs. Tóth, E. Esarey, K. Swanson, L. Fan-Chiang, G. Bagdasarov, N. Bobrova, V. Gasilov,

- G. Korn, P. Sasorov, and W. P. Leemans. Petawatt laser guiding and electron beam acceleration to 8 gev in a laser-heated capillary discharge waveguide. *Phys. Rev. Lett.*, 122:084801, Feb 2019. doi:10.1103/PhysRevLett.122.084801. URL <https://link.aps.org/doi/10.1103/PhysRevLett.122.084801>.
44. N. Tripathi, B. Miao, A. Sloss, E. Rockafellow, J. E. Shrock, S. W. Hancock, and H. M. Milchberg. Longitudinal shaping of plasma waveguides using diffractive axicons for laser wakefield acceleration. *Opt. Lett.*, 50(10):3441–3444, May 2025. doi:10.1364/OL.561318. URL <https://opg.optica.org/ol/abstract.cfm?URI=ol-50-10-3441>.
  45. C. G. Durfee and H. M. Milchberg. Light pipe for high intensity laser pulses. *Phys. Rev. Lett.*, 71:2409–2412, Oct 1993. doi:10.1103/PhysRevLett.71.2409. URL <https://link.aps.org/doi/10.1103/PhysRevLett.71.2409>.
  46. C. G. Durfee, J. Lynch, and H. M. Milchberg. Development of a plasma waveguide for high-intensity laser pulses. *Phys. Rev. E*, 51:2368–2389, Mar 1995. doi:10.1103/PhysRevE.51.2368. URL <https://link.aps.org/doi/10.1103/PhysRevE.51.2368>.
  47. S. Lorenz, G. Grittani, E. Chacon-Golcher, C. M. Lazzarini, J. Limpouch, F. Nawaz, M. Nevrla, L. Vilanova, and T. Levato. Characterization of supersonic and subsonic gas targets for laser wakefield electron acceleration experiments. *Matter and Radiation at Extremes*, 4(1):015401, 01 2019. ISSN 2468-2047. doi:10.1063/1.5081509. URL <https://doi.org/10.1063/1.5081509>.
  48. B. Miao, J. E. Shrock, E. Rockafellow, A. J. Sloss, and H. M. Milchberg. Meter-scale supersonic gas jets for multi-gev laser-plasma accelerators. *Review of Scientific Instruments*, 96(4):043003, 04 2025. ISSN 0034-6748. doi:10.1063/5.0248959. URL <https://doi.org/10.1063/5.0248959>.
  49. C. V. Pieronek, A. J. Gonsalves, C. Benedetti, S. S. Bulanov, J. van Tilborg, J. H. Bin, K. K. Swanson, J. Daniels, G. A. Bagdasarov, N. A. Bobrova, V. A. Gasilov, G. Korn, P. V. Sasorov, C. G. R. Geddes, C. B. Schroeder, W. P. Leemans, and E. Esarey. Laser-heated capillary discharge waveguides as tunable structures for laser-plasma acceleration. *Physics of Plasmas*, 27(9):093101, 09 2020. ISSN 1070-664X. doi:10.1063/5.0014961. URL <https://doi.org/10.1063/5.0014961>.
  50. B. Miao, L. Feder, J. E. Shrock, and H. M. Milchberg. Phase front retrieval and correction of bessell beams. *Opt. Express*, 30(7):11360–11371, Mar 2022. doi:10.1364/OE.454796. URL <https://opg.optica.org/oe/abstract.cfm?URI=oe-30-7-11360>.
  51. M. Turner, S. S. Bulanov, C. Benedetti, A. J. Gonsalves, W. P. Leemans, K. Nakamura, J. van Tilborg, C. B. Schroeder, C. G. R. Geddes, and E. Esarey. Strong-field qed experiments using the bella pw laser dual beamlines. *The European Physical Journal D*, 76(11):205, 2022. doi:10.1140/epjd/s10053-022-00535-y. URL <https://doi.org/10.1140/epjd/s10053-022-00535-y>.
  52. P. Boucher, J. Del Hoyo, C. Billet, O. Pinel, G. Labroille, and F. Courvoisier. Generation of high conical angle bessell-gauss beams with reflective axicons. *Appl. Opt.*, 57(23):6725–6728, Aug 2018. doi:10.1364/AO.57.006725. URL <https://opg.optica.org/ao/abstract.cfm?URI=ao-57-23-6725>.
  53. P. B. Corkum, N. H. Burnett, and F. Brunel. Above-threshold ionization in the long-wavelength limit. *Phys. Rev. Lett.*, 62:1259–1262, Mar 1989. doi:10.1103/PhysRevLett.62.1259. URL <https://link.aps.org/doi/10.1103/PhysRevLett.62.1259>.
  54. X. M. Tong and C. D. Lin. Empirical formula for static field ionization rates of atoms and molecules by lasers in the barrier-suppression regime. *Journal of Physics B: Atomic, Molecular and Optical Physics*, 38(15):2593, jul 2005. doi:10.1088/0953-4075/38/15/001. URL <https://doi.org/10.1088/0953-4075/38/15/001>.
  55. A. Alejo, J. Cowley, A. Picksley, R. Walczak, and S. M. Hooker. Demonstration of kilohertz operation of hydrodynamic optical-field-ionized plasma channels. *Phys. Rev. Accel. Beams*, 25:011301, Jan 2022. doi:10.1103/PhysRevAccelBeams.25.011301. URL <https://link.aps.org/doi/10.1103/PhysRevAccelBeams.25.011301>.
  56. C. M. Lazzarini, L. V. Goncalves, G. M. Grittani, S. Lorenz, M. Nevrla, P. Valenta, T. Levato, S. V. Bulanov, and G. Korn. Electron acceleration at eli-beamlines: Towards high-energy and high-repetition rate accelerators. *International Journal of Modern Physics A*, 34(34):1943010, 2019. doi:10.1142/S0217751X19430103. URL <https://doi.org/10.1142/S0217751X19430103>.
  57. T. Willemsen, U. Chaulagain, I. Havlíčková, S. Borneis, W. Ebert, H. Ehlers, M. Gauch, . Groß, D. Kramer, T. Laštovička, J. Nejd, B. Rus, K. Schrader, T. Tolenis, F. Vaněk, P. K. Velpula, and S. Weber. Large area ion beam sputtered dielectric ultrafast mirrors for petawatt laser beamlines. *Opt. Express*, 30(4):6129–6141, Feb 2022. doi:10.1364/OE.452249. URL <https://opg.optica.org/oe/abstract.cfm?URI=oe-30-4-6129>.
  58. J. M. Auerbach and V. P. Karpenko. Serrated-aperture apodizers for high-energy laser systems. *Appl. Opt.*, 33(15):3179–3183, May 1994. doi:10.1364/AO.33.003179. URL <https://opg.optica.org/ao/abstract.cfm?URI=ao-33-15-3179>.
  59. C. Iaconis and I. A. Walmsley. Spectral phase interferometry for direct electric-field reconstruction of ultrashort optical pulses. *Opt. Lett.*, 23(10):792–794, May 1998. doi:10.1364/OL.23.000792. URL <https://opg.optica.org/ol/abstract.cfm?URI=ol-23-10-792>.

60. T. M. Antonsen, Jr. and P. Mora. Leaky channel stabilization of intense laser pulses in tenuous plasmas. *Phys. Rev. Lett.*, 74:4440–4443, May 1995. doi:10.1103/PhysRevLett.74.4440. URL <https://link.aps.org/doi/10.1103/PhysRevLett.74.4440>.
61. T. R. Clark and H. M. Milchberg. Optical mode structure of the plasma waveguide. *Phys. Rev. E*, 61:1954–1965, Feb 2000. doi:10.1103/PhysRevE.61.1954. URL <https://link.aps.org/doi/10.1103/PhysRevE.61.1954>.